1088. Dynamics of mass-spring-belt friction self-excited vibration system

Xiaopeng Li[1], Guanghui Zhao[2], Xing Ju[3], Yamin Liang[4], Hao Guo[5]

[1, 2, 3, 4]School of Mechanical Engineering and Automation, Northeastern University, China
[5]Zhengzhou Yutong Bus Co., Ltd., Henan Province, China
E-mail: [1]*xpli@me.neu.edu.cn*, [2]*zghedu2012@163.com*, [3]*juxing_neu@163.com*,
[4]*liangyamin1127@126.com*, [5]*gh410521@163.com*

Abstract. In order to deeply study the non-smooth dynamic mechanism of self-excited vibration, the friction self-excited vibration system model containing the Stribeck friction model is established, which is a nonlinear dynamical mass-spring-belt model. For the established model, the critical instability speed is solved by the first approximate stability criterion of Lyapunov theory, and the stability of limit cycle is determined on the basis of curvature coefficient. Secondly, the bifurcation characteristics and system behaviors under different parameters are analyzed by using numerical simulation method. The results show that the theoretical analysis is feasible. Feed speed, damping coefficient and ratio of dynamic-static friction coefficient are the main factors that affect the system motion state. Thirdly, the Washout filter method is designed to control the bifurcation characteristics. By comparing the pre and post phase diagrams, results show that the amplitude of controlled system is reduced and the topology is improved after introducing the Washout filter. All the researches above prove that adding Washout filter into the system to control the bifurcation phenomenon is a more effective method.

Keywords: self-excited vibration, friction model, bifurcation control, stability.

1. Introduction

The friction-induced vibration phenomenon exists widely in the engineering field and daily life, and affects the performance of the mechanical system in various ways. The friction-induced vibration problems usually cause mechanical parts to wear and then reduce the precision and quality of workpiece. Besides they can also reduce the precision of control system. So many scholars have carried out a lot of studies on the modeling of friction system and system dynamics. On the aspect of modeling, people have established a series of friction models, such as Coulomb friction model [1], Stribeck friction model [2], Karnopp friction model [3], Dahl friction model [4] and Lu Gre friction model [5]. On the aspect of system dynamics, Feeny [6] studied the chaotic behavior of oscillator containing dry friction by the comparison of experiment and simulation. Ding [7] investigated the nonlinear dynamic characteristics of a vibration system affected by dry friction. In order to capture dividing points accurately, the theoretical method about the points which separate slip phases from stick phases is expounded. The stick-slip vibration is analyzed and the Lyapunov exponent is used to investigate the stability of the system. Gdaniec [8] researched single-freedom friction oscillator by using Lu Gre friction model. He found different feed speeds and friction coefficients could cause the friction-induced bifurcation and chaotic phenomenon. Madeleine [9] studied the frictional excitation characteristics of single-freedom mass-damping-spring system under the condition of interval load.

While researches considering the friction of mechanical system dynamics have a long history, but so far the mechanism of the non-smooth dynamics including the self-excited vibration has not yet been deeply understood, the research theory of the self-excited vibration lacks of systemic. The damping of high-speed train [10], flutter of aircraft wing [11], vibration of high-speed cutting [12] and oil whipping of turbogenerator [13] are all related to self-excited vibration. So studies on dynamic characteristics of self-excited vibration have important significance on theoretical and practical applications. Therefore this paper takes the representative machine tool cutting system and feed system as the research object, the dynamics and bifurcation control of friction self-excited

vibration phenomenon are deeply researched. All the work in this paper has certain reference value on the dynamic characteristics of friction self-excited vibration system.

2. Stability analysis of friction self-excited vibration system

Modeling accurately for the important friction phenomenon is a familiar research method. For the self-excitation vibration mechanism, scholars at home and abroad have established some models, which can explain the phenomenon to some extent. But the application situations of these models are different from each other and these models have many disadvantages themselves:

(1) It is uneasy to construct the mathematical model, which brings difficulties to do the mathematical analysis of crawling;

(2) It is difficult to realize the dynamic numerical simulation analysis;

(3) The previous studies are just concentrated on the experiment and mainly study the effect of feed speed on the dynamic system. While the effects of damping coefficient, transmission stiffness and dynamic and static friction coefficients are merely concerned;

(4) Normal load is often hypothesized as a constant in the completed researches. However actually, because of the surface roughness and waviness, the moving parts often make system up and down in the vertical direction. So vibration exists in the vertical direction of coordinate system.

So a simple model is needed to make deep study. Considering systematic changes have direct relationships with the mass, stiffness, damping, friction coefficient and normal vibration, the mass-spring-belt self-excited vibration system model is established in Figure 1.
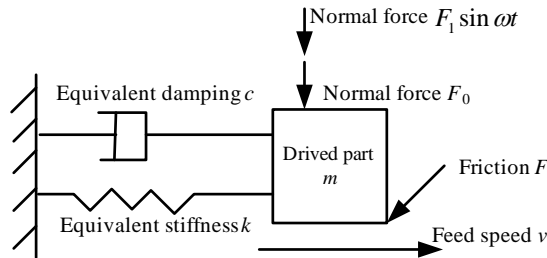

Fig. 1. The mechanical model of the mass-spring-belt system

The dynamic equation of the system is:

$$m\frac{d^2x}{dt^2} + c\frac{dx}{dt} + kx - F = 0. \tag{1}$$

Then the dimensionless expression is:

$$\ddot{X} + 2\beta\dot{X} + X - \mu = 0, \tag{2}$$

where $F = N\mu$, $\omega_0 = \sqrt{k/m}$, $\tau = \omega_0 t$, $X = xk/N$, $2\beta = c\omega/k$, $v_0 = \frac{v_0}{\omega_0 L}$, $\Omega = \frac{\tilde{\Omega}}{\omega_0}$.

The Stribeck friction model is introduced in this paper. This model is very classical and can describe the general friction behavior of joint surfaces of mechanical movement of parts. The expression of the model is:

$$\mu = -\mu_s sgn\left(\frac{dX}{d\tau} - v_0\right) + \frac{3(\mu_s - \mu_m)}{2v_m}\left(\frac{dX}{d\tau} - v_0\right) - \frac{(\mu_s - \mu_m)}{2v_m^3}\left(\frac{dX}{d\tau} - v_0\right)^3, \tag{3}$$

where $\dot{X} = dX/d\tau$ is the non-dimensional speed, v_0 is the belt speed, v_m is the speed that

corresponds to the minimum dynamic friction, μ_s is dynamic friction coefficient, μ_m is the static friction coefficient.

Based on the theory of ordinary differential equations, the higher order differential equation can be transformed into first order differential equations. The equivalent transformation is made as:

$$\begin{cases} X = X_1, \\ \dfrac{dX}{d\tau} = X_2. \end{cases} \tag{4}$$

Then the Equation (3) can be transformed into first order differential equations:

$$\begin{cases} \dfrac{dX_1}{d\tau} = X_2, \\ \dfrac{dX_2}{d\tau} = -2\beta X_2 - X_1 - \mu_s \operatorname{sgn}\left(\dfrac{dX}{d\tau} - v_0\right) + \dfrac{3(\mu_s - \mu_m)}{2v_m}\left(\dfrac{dX}{d\tau} - v_0\right) - \dfrac{\mu_s - \mu_m}{2v_m^3}\left(\dfrac{dX}{d\tau} - v_0\right)^3. \end{cases} \tag{5}$$

Based on the reference [14], when the input speed of the system is very fast, the mass block is in the condition of static balance under the effect of friction force and spring force. In this condition $\ddot{X} = 0$, $\dot{X} = 0$, $\operatorname{sgn}(v_r) = -1$. When $\mu_s = 0.4$, $\mu_m = 0.25$, $v_m = 0.5$, the stability of balance point can be analysed by Lyapunov stability theory.

When $\frac{dX_i}{d\tau} = 0$ in Equation (5), the equilibrium point of the system is solved as:

$$\begin{cases} X_{20} = 0, \\ X_{10} = \mu = 0.4 - 0.45v_0 + 0.6v_0^3, \end{cases} \tag{6}$$

where $\begin{cases} X_1 = \bar{X}_1 + X_{10}, \\ X_2 = \bar{X}_2 + X_{20}, \end{cases} \begin{cases} F_1 = 0, \\ F_2 = -0.45\bar{X}_2 + 0.6(\bar{X}_2^3 + 3\bar{X}_2 v_r^2 - 3\bar{X}_2^2). \end{cases}$

The first approximate equation is obtained after expanding the Equation (5) into Taylor series and dropping the quadratic term. For the first approximate equation, the jacobian matrix of variables X_1 and X_2 can be expressed as Equation (7) when $X_1 = 0$ and $X_2 = 0$:

$$A = \begin{bmatrix} 0 & 1 \\ a_{21} & a_{22} \end{bmatrix} = 0. \tag{7}$$

When dimensionless damping coefficient $\beta = 0.01$, the characteristic equation of matrix A is:

$$|\lambda E - A| = \begin{vmatrix} \lambda & 1 \\ -1 & \lambda - (0.45 - \beta - 1.8v_0^2) \end{vmatrix} = \lambda^2 - (0.44 - 1.8v_0^2)\lambda + 1 = 0. \tag{8}$$

For the certain driving velocity v_0, the equilibrium point and its corresponding eigenvalue can be obtained by the Equation (6) and Equation (8). Based on the Hurwits law, the critical instability speed of system can be solved by $p = 0.44 - 1.8v_0^2 = 0$. In this condition $v_{b1} = 0.4944$ is the supercritical Hopf bifurcation point.

The amplitude approximate solution of limit cycle in multi-dimensional system has pointed that curvature coefficient is an important basis to determine the stability of limit cycle. Regarding the Hopf bifurcation characteristics as the starting point, this paper gets the Jordan standard form by proper linear transform and deduces the expression of curvature coefficient of limit cycle by centre manifold theory [14]. So in order to judge the stability of limit cycle, the linear transformation is taken into the standard form in Equation (5):

$$\dot{Y} = AY + Q, \tag{9}$$

where $A = \begin{bmatrix} 0 & 1 \\ -1 & 0.44 - 1.8v_0^2 \end{bmatrix}$, $Q = \begin{cases} Q_1, \\ Q_2, \end{cases} = \begin{cases} 0, \\ 1.8v_0 y_2^2 - 0.6y_2^3. \end{cases}$

Based on the Equation (6), the equilibrium point is $(y, \dot{y}) = (0, 0.4 - 0.45v_0 + 0.6v_0^3)$. And the eigenvalues of Equation (7) are:

$$\lambda_{1,2} = \alpha(v_0) \pm \beta(v_0), \tag{10}$$

where $\alpha(v_0) = (0.44 - 1.8v_0^2)/2$, $\beta(v_0) = \sqrt{(0.44 - 1.8v_0^2)^2 - 4}/2$.

When $\alpha(v_0) = (0.44 - 1.8v_0^2)/2 = 0$:

$$\alpha'(0) = ((0.44 - 1.8v_0^2)/2)'|_{v_0 = v_{b1}} = -3.6 \times 0.4944 = -1.7798 < 0, \tag{11}$$

$$g_{20} = \frac{1}{4}\left(\frac{\partial^2 Q_1}{\partial y_1^2} - \frac{\partial^2 Q_1}{\partial y_2^2} + 2\frac{\partial^2 Q_1}{\partial y_1 \partial y_2} + i\left(\frac{\partial^2 Q_2}{\partial y_1^2} - \frac{\partial^2 Q_2}{\partial y_2^2} - 2\frac{\partial^2 Q_1}{\partial y_1 \partial y_2}\right)\right) = -\frac{1.7788}{4}i, \tag{12}$$

$$g_{11} = \frac{1}{4}\left(\frac{\partial^2 Q_1}{\partial y_1^2} + \frac{\partial^2 Q_1}{\partial y_2^2} + i\left(\frac{\partial^2 Q_2}{\partial y_1^2} + \frac{\partial^2 Q_2}{\partial y_2^2}\right)\right) = \frac{1.7788}{4}i, \tag{13}$$

$$G_{21} = \frac{1}{8}\left(\frac{\partial^3 Q_1}{\partial y_1^3} + \frac{\partial^3 Q_1}{\partial y_1 \partial y_2^2} + \frac{\partial^3 Q_2}{\partial y_1^2 \partial y_2} + \frac{\partial^3 Q_2}{\partial y_2^3} + i\left(\frac{\partial^3 Q_2}{\partial y_1^3} - \frac{\partial^3 Q_2}{\partial y_1 \partial y_2^2} - 2\frac{\partial^3 Q_1}{\partial y_1^2 \partial y_2}\right)\right)$$
$$= -\frac{3.6}{8}. \tag{14}$$

Based on the Equation (12), Equation (13) and Equation (14), the curvature coefficient of limit cycle is:

$$\sigma_1 = \text{Re}\left\{\frac{g_{20}g_{11}}{2\omega_0}\right\} \text{Re}\left\{-\frac{3.6}{16} + \frac{1.7788^2}{16}i\right\} = -\frac{3.6}{16} < 0. \tag{15}$$

When $\sigma_1 < 0$ and $\alpha'(0) < 0$, the bifurcation of system is generated in the point of $v = v_{b1}$. In the direction of $v < v_{b1}$ the limit cycle is in a stable status, while the equilibrium point is in an unstable state.

When the feed speed $v_0 = 0.45 < v_{b1}$, the criterion conditions of stability are: $\Delta = p^2 - 4q < 0$, $p > 0$. Then the eigenvalues of the equation do not have negative real parts. The equilibrium point is an unstable focus and produces the limit cycle which tends to be stable. So the ultimate motion is periodic motion and can be divided into two types: the pure sliding vibration where the stick-slip vibration of the mass block never occurred and the stick-slip vibration where the mass block is viscous on the belt on occasion.

When the feed speed $v_0 = 0.495 > v_{b1}$, the criterion conditions of stability are: $\Delta = p^2 - 4q < 0$, $p < 0$. Then the eigenvalues of the equation have negative real parts. The equilibrium point is a stable focus and the solution of equation is gradually attenuating to zero. So the ultimate motion is stable.

3. Numerical simulation of friction self-excited vibration system

3.1. Bifurcation numerical simulation

Hopf bifurcation is that the equilibrium point changes from stable focus into unstable focus when the parameters pass by the critical point. It is an important dynamic bifurcation problem and has a close relation with the generation of self-excited vibration in engineering.

When $\mu_s = 0.4$, $\mu_m = 0.25$, $v_m = 0.5$ and $\gamma = 1$, the bifurcation diagram can be studied with feed speed, damping coefficient, transmission stiffness and ratio of dynamic and static friction coefficients as bifurcation parameters. The results are shown in Figures 2-5.

From the Figure 2, in the system begins to appear bifurcation phenomenon and the equilibrium point changes from stable focus into unstable focus when the feed speed reaches 0.4944. Then the limit cycle disappears and the system tends to be stable. The bifurcation diagram can be divided into quasi-periodic motion area ($0 < v_0 < 0.4944$) and single-value curves area ($0.4944 < v_0 < 1$). The results show that when v_0 reaches the critical velocity v_{b1}, the stable limit cycle produced by self-excited vibration is changed into stable state. That is to say the system is in the quasi-periodic motion state at a low feed speed and tends to be stable when the speed is high to a certain degree. All the research above verify the feasibility of the stability analysis.
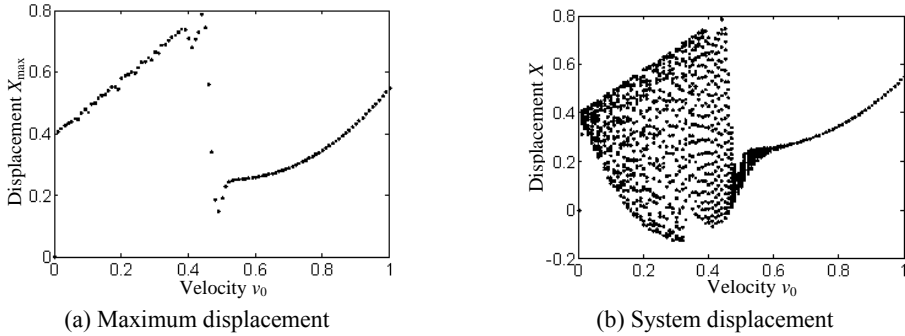

(a) Maximum displacement   (b) System displacement

Fig. 2. The system bifurcation diagram with the feed speed as the bifurcation parameter

(a) Maximum displacement   (b) System displacement
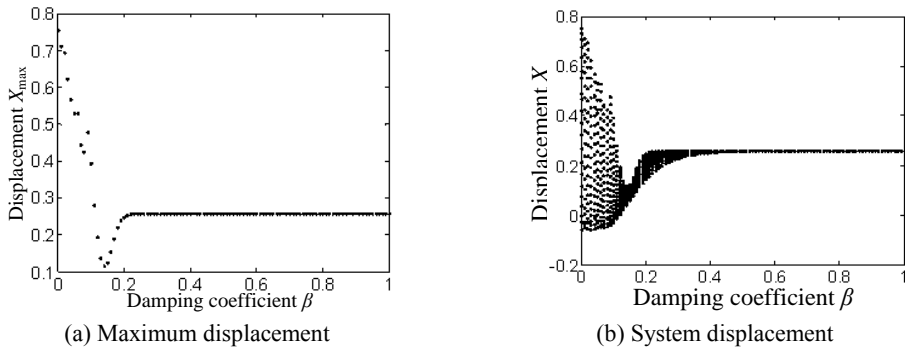
Fig. 3. The system bifurcation diagram with the damping coefficient as the bifurcation parameter

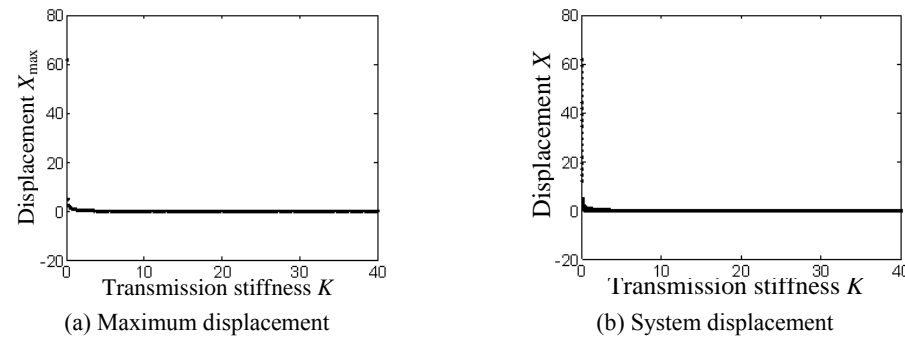(a) Maximum displacement   (b) System displacement

Fig. 4. The system bifurcation diagram with the transmission stiffness as the bifurcation parameter

Likewise, from the Figure 3 the quasi-periodic motion ($0 < \beta < 0.02$) has occurred mainly in

small damping coefficient region. The system will be stable when the damping coefficient is high to a certain degree. From the Figure 4 the influence of transmission stiffness on the system characteristics is not so great. Only increasing transmission stiffness will not inhibit the self-excited vibration. From the Figure 5 larger ratio of dynamic and static friction coefficients leads to the phenomenon of self-excited vibration. Inversely, the stable state occurs in a small ratio of dynamic and static friction coefficients.
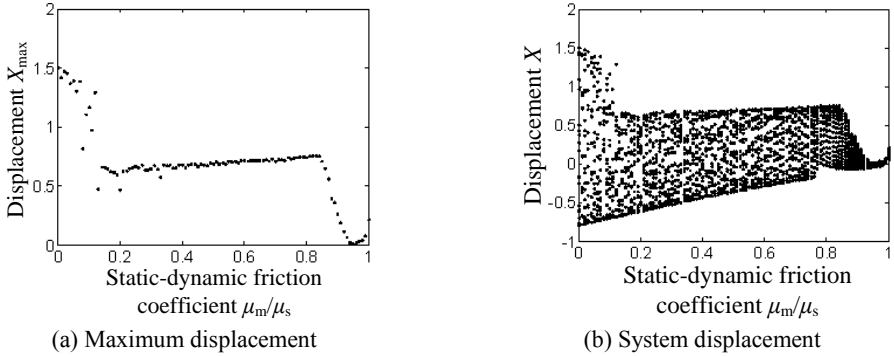

(a) Maximum displacement

(b) System displacement

Fig. 5. The system bifurcation diagram with the ratio of dynamic and static friction coefficients as the bifurcation parameter

3.2. Numerical simulation under different feed speeds

When $\beta = 0.01$, $\mu_s = 0.4$, $\mu_m = 0.25$, $v_m = 0.5$, $\gamma = 1$ and the initial conditions are $X = 0$, $\dot{X} = 0$, the phase diagrams under different feed speeds are shown in Figure 6, where $v_{b1} = 0.4944$, $v_{b0} = 0.4372$.
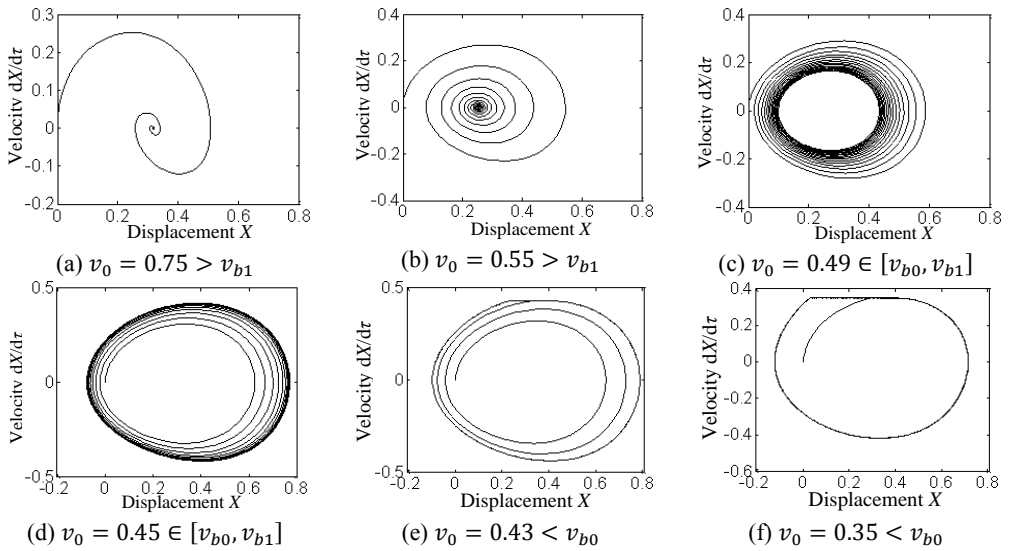

(a) $v_0 = 0.75 > v_{b1}$

(b) $v_0 = 0.55 > v_{b1}$

(c) $v_0 = 0.49 \in [v_{b0}, v_{b1}]$

(d) $v_0 = 0.45 \in [v_{b0}, v_{b1}]$

(e) $v_0 = 0.43 < v_{b0}$

(f) $v_0 = 0.35 < v_{b0}$

Fig. 6. The phase diagrams under the action of different feed speeds

From the Figure 6, system motion can be divided into three stages when feed speed changes between critical velocities. When the feed speed is $v_0 > v_{b1} = 0.4944$, the system will be stabilized at the equilibrium point. Then the relative velocity is the feed speed. The time tending to be stable decreased with the feed speed increased. That is to say, the bigger the feed speed the better stability it has. In the equilibrium point of system occurs instability and it begins to cause

self-excited vibration when the feed speed is $v_0 < v_{b1}$. The process can be further divided into pure slip ($v_{b0} < v_0 < v_{b1}$) where in the phase diagram does not exist limit cycle and the minimum relative speed between mass block and belt is not zero, and stick slip ($v_0 < v_{b0} = 0.4372$) where the limit cycle has obvious viscous stage and the minimum relative speed between mass block and belt is zero. When the minimum relative speed is zero, the input speed is the demarcation point translated from pure slip into stick slip.

3.3. Numerical simulation under different damping coefficients

System damping has important influence on the whole motion. And it can prevent the occurrence of vibration when the damping satisfies certain conditions. Based on the Equation (8), the critical velocity can be solved by $p = 0$ for the specific damping coefficient β.

When $\mu_s = 0.4$, $\mu_m = 0.25$, $v_m = 0.5$, $\gamma = 1$ and the initial conditions are $X = 0$, $\dot{X} = 0$, the phase diagrams under different damping coefficients are shown in Figure 7. Changing the Stribeck friction model as Coulomb friction model, the phase diagrams under different damping coefficients are shown in Figure 8. Likewise, when the friction model is linear friction model ($\mu = -\mu_s \mathrm{sgn} v_r + 3(\mu_s - \mu_m)v_r/v_m$), the phase diagrams under different damping coefficients are shown in Figure 9.
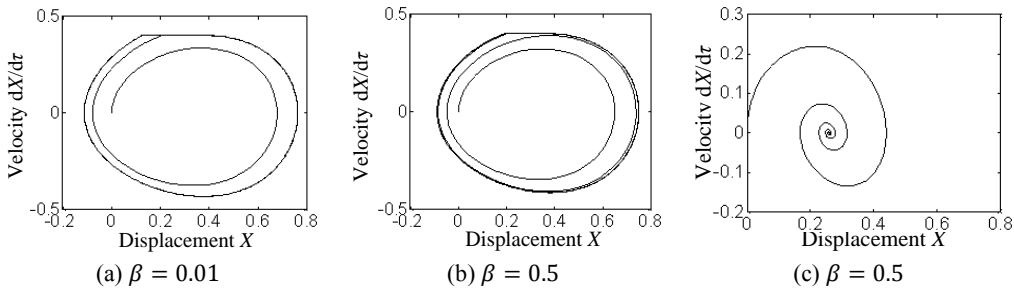

(a) $\beta = 0.01$　　　　　(b) $\beta = 0.5$　　　　　(c) $\beta = 0.5$

Fig. 7. The phase diagrams under different damping coefficients

(a) $\beta = 0$　　　　　(b) $\beta = 0.2$　　　　　(c) $\beta = 0.8$
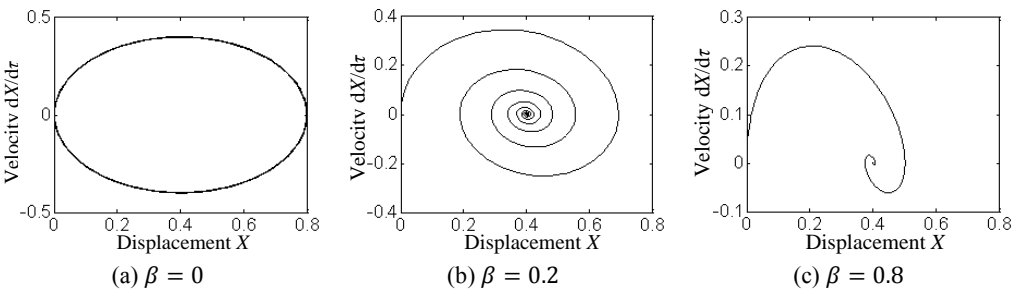
Fig. 8. The phase diagrams under different damping coefficients

(a) $\beta = 0$　　　　　(b) $\beta = 0.2$　　　　　(c) $\beta = 0.8$
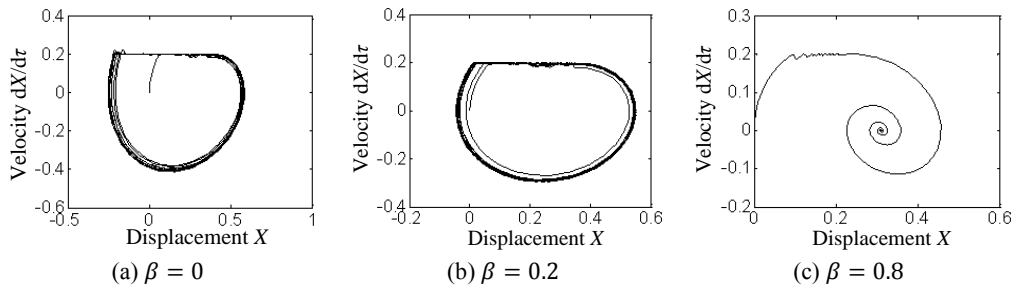
Fig. 9. The phase diagrams under different damping coefficients

From the Figure 7, the proportion of viscous stage decreased with the increase of damping. When the damping is great to a certain degree, the viscous stage disappears and the system begins stable pure slip motion. Continuing increase of the damping to the critical value, the system will be stable at the equilibrium point. So increasing damping to a certain extent can inhibit the self-excited vibration and improve the stability of the system. Comparing the Figure 8 with Figure 9, when the friction model is linear friction model where the relationship between friction and speed is with negative slope, self-induced vibration occurs in the system. And the proportion of viscous stage decreased with the increase of damping. The results show that negative friction-speed slope is the main cause of self-induced vibration.

3.4. Numerical simulation under different transmission stiffness

Transmission stiffness has important influence on the whole motion. Based on the stability theoretical analysis above, transmission stiffness has the function of improving the stability of system. When $\mu_s = 0.4$, $\mu_m = 0.25$, $v_m = 0.5$, $\gamma = 1$, $\beta = 0.01$, $v_0 = 0.2$ and the initial conditions are $X = 0$, $\dot{X} = 0$, the phase diagrams under different transmission stiffnesses are shown in Figure 10.
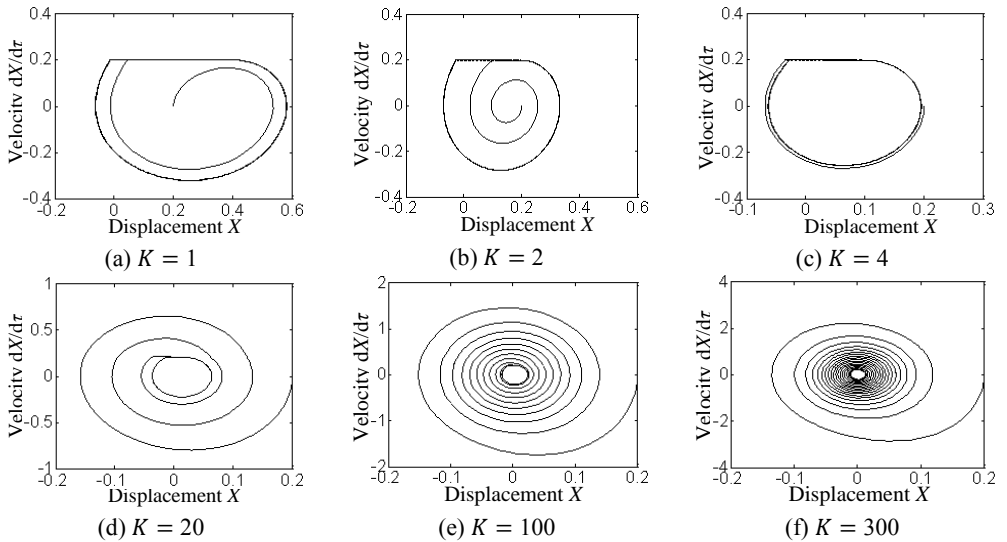

(a) $K = 1$ (b) $K = 2$ (c) $K = 4$

(d) $K = 20$ (e) $K = 100$ (f) $K = 300$

Fig. 10. The phase diagrams under different transmission stiffnesses

From the Figure 10, the proportion of viscous stage decreased with the increase of transmission stiffness. When the transmission stiffness is great to a certain degree, the viscous stage disappears and the system begins stable pure slip motion. And the limit cycle decreased with the increase of stiffness. So increasing stiffness to a certain extent can shorten viscous stage and improve the stability of the system.

3.5. Numerical simulation under different dynamic and static friction coefficients

When $\beta = 0.01$, $\mu_s = 0.4$, $\mu_m = 0.25$, $v_m = 0.5$, $\gamma = 1$ and the initial conditions are $X = 0$, $\dot{X} = 0$, the phase diagrams under different dynamic and static friction coefficients are shown in Figure 11.

From the Figure 11, vibration amplitude of the system and the proportion of viscous stage increased with the increase of gap of dynamic and static friction coefficients. When the gap of dynamic and static friction coefficients is decreased to a certain degree, the viscous stage

disappears and the system begins stable pure slip motion. Continuing decrease of the gap, the system will be stable and no longer performing vibration.
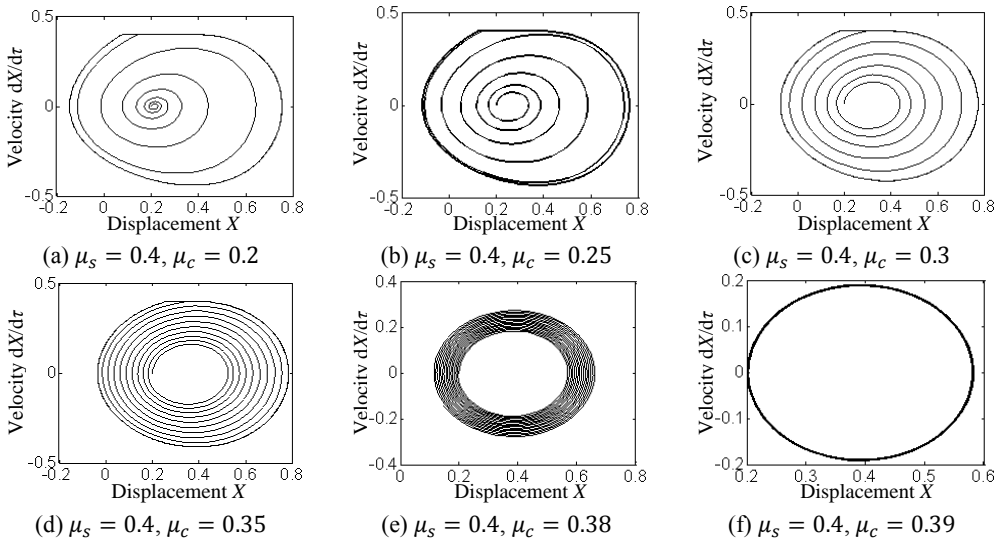

(a) $\mu_s = 0.4$, $\mu_c = 0.2$ (b) $\mu_s = 0.4$, $\mu_c = 0.25$ (c) $\mu_s = 0.4$, $\mu_c = 0.3$

(d) $\mu_s = 0.4$, $\mu_c = 0.35$ (e) $\mu_s = 0.4$, $\mu_c = 0.38$ (f) $\mu_s = 0.4$, $\mu_c = 0.39$

Fig. 11. The phase diagrams under the difference of dynamic and static friction coefficients

4. Bifurcation control of friction self-excited vibration system

4.1. Design of Washout filter and the stability analysis

When the feed speed is 0.48, 0.49 and 0.492, the dynamic characteristics of friction self-excited vibration can be obtained and the phase diagrams are shown in Figure 12.
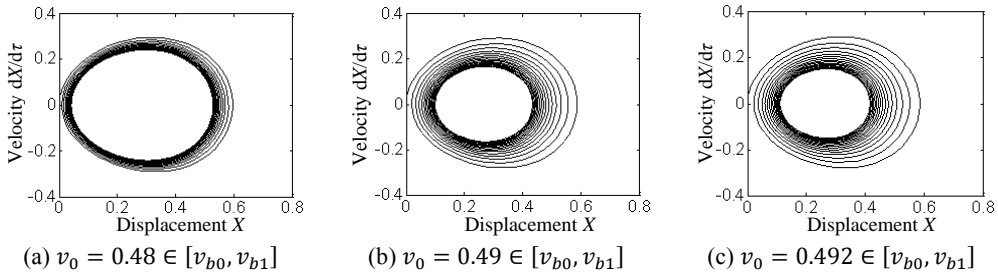

(a) $v_0 = 0.48 \in [v_{b0}, v_{b1}]$ (b) $v_0 = 0.49 \in [v_{b0}, v_{b1}]$ (c) $v_0 = 0.492 \in [v_{b0}, v_{b1}]$

Fig. 12. The phase diagrams under the action of different feed speeds

From the Figure 12, when the feed speed is greater than or equal to 0.49, amplitude of the limit cycle becomes suddenly decreased and the equilibrium point is in an unstable state. In the process of decreasing the feed speed, the limit cycle changed from stable into unstable and the equilibrium point changed from unstable into stable. Based on the stability analysis, in the system occurs the subcritical bifurcation when speed passes by the point of 0.49. To decrease the amplitude, Washout filter is introduced to control the bifurcation [15].

When the friction is linear, the friction self-excited vibration system can be expressed as:

$$\begin{cases} \dot{x} = y, \\ \dot{y} = -F - Cy - Kx, \end{cases} \tag{16}$$

where $F = -0.45\bar{X}_2 + 0.6(\bar{X}_2^3 + 3\bar{X}_2 v_r^2 - 3\bar{X}_2^2)$.

To control y with Washout filter, the control system can be expressed as:

$$\begin{cases} \dot{x} = y, \\ \dot{y} = -F - Cy - Kx, \\ \dot{\omega} = y - d\omega. \end{cases} \tag{17}$$

The controller can be designed as the form of:

$$u = g(v; K) = k_1 v + k_2 v^3, \tag{18}$$

where $K = (k_1, k_2)$ is the control vector, k_1 is the linear gain, k_2 is non-linear gain. The linear part can control the production of Hopf bifurcation, the cubic term can control the amplitude of the limit cycle.

Taking Equation (17) into Equation (18), the system can be expressed as Equation (19):

$$\begin{cases} \dot{x} = y, \\ \dot{y} = -F - Cy - Kx + k_1(y - d\omega) + k_2(y - d\omega)^3, \\ \dot{\omega} = y - d\omega. \end{cases} \tag{19}$$

The Jacobian matrix of the linear part of the system is:

$$J = \begin{bmatrix} 0 & 1 & 0 \\ -1 & 0.0078 + k_1 & -2k_1 \\ 0 & 1 & -2 \end{bmatrix}. \tag{20}$$

The characteristic equation of the Jacobian matrix is:

$$\lambda^3 + c_1\lambda^2 + c_2\lambda + c_3 = 0, \tag{21}$$

where $c_1 = 2 - (0.44 - 1.8v_0^2 + k_1)$, $c_2 = 2k_1 - (0.44 - 1.8v_0^2 + 1)$, $c_3 = 2$.

Based on the Routh-Hurwits criterion $c_1c_2 = c_3$, that is to say $k_1 = -0.0395$ is the condition of Hopf bifurcation. The amplitude of limit cycle can be regulated by changing the value of k_2.

The characteristic roots of Equation (21) are $\lambda_{1,2} = \alpha(v_0) \pm \beta(v_0)$ and $\lambda_3 = c$, where $\alpha(v_0) = -(1.5995 + 1.8v_0^2) + O(v_0^2)$ and:

$$\alpha'(0) = \left(-(1.5995 + 1.8v_0^2)\right)' \Big|_{v_0=0.49} = -3.6 \times 0.49 = -1.764 < 0. \tag{22}$$

When $v_0 = 0.49$, the characteristic quantities are:

$$g_{20} = \frac{1}{4}\left(\frac{\partial^2 Q_1}{\partial y_1^2} - \frac{\partial^2 Q_1}{\partial y_2^2} + 2\frac{\partial^2 Q_1}{\partial y_1 \partial y_2} + i\left(\frac{\partial^2 Q_2}{\partial y_1^2} - \frac{\partial^2 Q_2}{\partial y_2^2} - 2\frac{\partial^2 Q_1}{\partial y_1 \partial y_2}\right)\right) = -\frac{1.764}{4}i, \tag{23}$$

$$g_{11} = \frac{1}{4}\left(\frac{\partial^2 Q_1}{\partial y_1^2} + \frac{\partial^2 Q_1}{\partial y_2^2} + i\left(\frac{\partial^2 Q_2}{\partial y_1^2} + \frac{\partial^2 Q_2}{\partial y_2^2}\right)\right) = \frac{1.764}{4}i, \tag{24}$$

$$G_{110} = \frac{1}{2}\left(\frac{\partial^2 Q_1}{\partial y_1 \partial y_3} + \frac{\partial^2 Q_2}{\partial y_1 \partial y_3} + i\left(\frac{\partial^2 Q_2}{\partial y_1 \partial y_3} - \frac{\partial^2 Q_1}{\partial y_1 \partial y_3}\right)\right) = 0, \tag{25}$$

$$G_{101} = \frac{1}{2}\left(\frac{\partial^2 Q_1}{\partial y_1 \partial y_3} - \frac{\partial^2 Q_2}{\partial y_1 \partial y_3} + i\left(\frac{\partial^2 Q_2}{\partial y_1 \partial y_3} + \frac{\partial^2 Q_1}{\partial y_1 \partial y_3}\right)\right) = 0, \tag{26}$$

$$w_{20} = \frac{1}{4\left(2i\omega(\mu_0 - \lambda_3(\mu_0))\right)}\left(\frac{\partial^2 Q_3}{\partial y_1^2} - \frac{\partial^2 Q_3}{\partial y_2^2} - 2i\frac{\partial^2 Q_3}{\partial y_1 \partial y_3}\right) = 0, \tag{27}$$

$$w_{11} = \frac{1}{4\lambda_3(\mu_0)}\left(\frac{\partial^2 Q_3}{\partial y_1^2} + \frac{\partial^2 Q_3}{\partial y_2^2}\right) = 0, \tag{28}$$

$$G_{21} = \frac{1}{8}\left(\frac{\partial^3 Q_2}{\partial y_2^3}\right) = \frac{1}{8}(6k_3 - 3.6). \tag{29}$$

According to the Equation (23) to Equation (29), the curvature coefficient of limit cycle is:

$$\sigma_1 = \text{Re}\left\{\frac{g_{20}g_{11}}{2\omega_0} + \frac{G_{21} + G_{101}g_{20}}{2}\right\} = \text{Re}\left\{\frac{1}{8}(6k_3 - 3.6) + \frac{3.6^2}{16}i\right\} = \frac{1}{8}(6k_3 - 3.6). \tag{30}$$

It can be seen obviously $\sigma_1 < 0$ when $k_3 < 0.6$. Based on $\sigma_1 < 0$ and $\alpha'(0) < 0$, in the system will occur Hopf bifurcation at the point of $v = 0.49$ and the bifurcation direction is $v < 0.49$.

4.2. Simulation analysis verification of bifurcation control

Before introducing the Washout filter, the Hopf supercritical bifurcation happens in the equilibrium point. Based on the bifurcation diagram with feed speed as the bifurcation parameter given above, the amplitude of the system changes remarkably and increases suddenly when the feed speed reduces approximately to 0.49. That is to say the subcritical bifurcation has happened.

After introducing the Washout filter, the Hopf supercritical bifurcation still happens in the equilibrium point. But the amplitude of system decreases when $v_0 = 0.49$. This shows that subcritical bifurcation is controlled.

When $v_0 = 0.4$, the phase diagrams are obtained after introducing the Washout filter at different values of k_1 and k_2, they are shown in Figure 13.

(a) $k_1 = -0.0395, k_2 = -0.01$　　(b) $k_1 = -0.0395, k_2 = -0.4$　　(c) $k_1 = -0.0395, k_2 = -0.8$
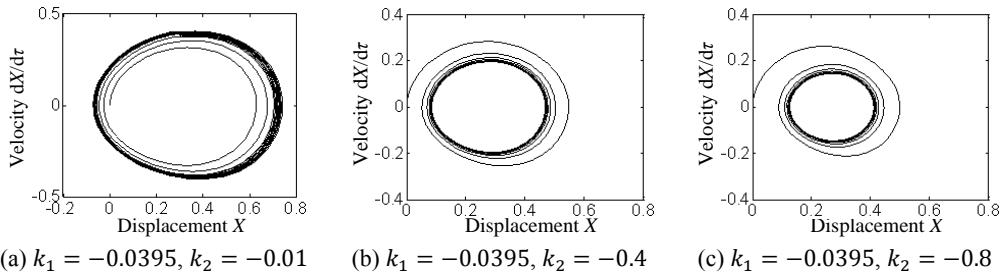
Fig. 13. The phase diagrams of the controlled system at different parameters

From the Figure 13, adjusting the parameters of controller can change the amplitude of self-induced vibration and make the limit cycle disappear. The Hopf bifurcation is well controlled. The results show that the Washout filter control designed above is reasonable.

5. Conclusions

Based on the dynamic characteristics analysis of friction vibration structure, the friction self-excited vibration system model containing the Stribeck model is established. For the certain feed speed, the equilibrium point of the system is solved and the equilibrium stability is analyzed by making use of the first approximate stability criterion of Lyapunov theory.

By the bifurcation numerical simulation and the numerical simulation under different

parameters of the system, stability analysis is verified feasible. The simulation results show that great feed speed and damping coefficient and low gap of dynamic and static friction coefficients can inhibit the self-excited variation to some extent. The research work of this paper has certain reference value on the dynamics characteristics of the self-excited vibration system in actual production.

The Washout filter method is introduced to control the Hopf bifurcation of friction self-excited vibration. By comparing the pre and post phase diagrams, results show that the amplitude of controlled system is reduced and the topology is improved after introducing the Washout filter. So the Washout filter control is a comparatively effective method to control the bifurcation of friction system.

Acknowledgement

References

[1] **Den Hartog J. P.** Forced vibration with combined Coulomb and viscous friction. Transactions of the ASME, APM, Vol. 53, Issue 9, 1997, p. 107-115.
[2] **Li Chun Bo, Pavelescu D.** The friction-speed relation and its influence on the critical velocity of the stick-slip motion. Wear, Vol. 82, Issue 3, 1982, p. 277-289.
[3] **Karnopp D.** Computer simulation of stick slip friction in mechanical dynamic systems. ASME Journal of Dynamic Systems, Measurement and Control, Vol. 107, Issue 1, 1985, p. 100-103.
[4] **Dahl P. R.** Measurement of solid friction parameters of ball bearings. Proceedings of the 6th Annual Symposium on Incremental Motion Control Systems and Devices, 1977, p. 49-60.
[5] **Canudas De Wit C., Olsson H., Astrom K. J., Lischinsky P.** A new model for control of systems with friction. IEEE Transactions on Automatic Control, Vol. 40, Issue 3, 1995, p. 419-425.
[6] **Feeny B., Moon F. C.** Chaos in a forced dry-friction oscillator: experiments and numerical modeling. Journal of Sound and Vibration, Vol. 170, Issue 3, 1994, p. 303-323.
[7] **Wangcai Ding, Youqiang Zhang, Qingshuang Zhang** Nonlinear dynamic analysis of vibrate system with dry friction. Engineering Mechanics, Vol. 25, Issue 10, 2008, p. 212-217.
[8] **Gdaniec P., Weiss C., Hoffmann N. P.** On chaotic friction induced vibration due to rate dependent friction. Mechanics Research Communications, Vol. 37, Issue 1, 2010, p. 92-95.
[9] **Pascal M.** New limit cycles of dry friction oscillators under harmonic load. Nonlinear Dynamics, Vol. 70, Issue 2, 2012, p. 1435-1443.
[10] **Caihong Huang** Study on Vibration Reduction Technologies for High Speed Cars. Chengdu, Southwest Jiaotong University, 2012.
[11] **Fayou Yang, Zhongquan Gu** Adaptive flutter suppression for aircraft wing. Journal of Nanjing University of Aeronautics & Astronautics, Vol. 36, Issue 6, 2004, p. 708-712.
[12] **Sinan Badrawy** Cutting dynamics of high speed machining. WolfTracks, Vol. 81, 2001, p. 24-26.
[13] **Kucherenko V. V., Gomez-Mancilla J. C.** Bifurcations of an exactly solvable model of rotor dynamics. International Journal of Bifurcation and Chaos in Applied Sciences and Engineering, Vol. 10, Issue 12, 2000, p. 2689-2699.
[14] **Suhua Liu** Feedback Control of Hopf Bifurcation in Two Classes of Nonlinear High Dimensional Systems. Changsha, Hunan University, 2008.
[15] **Jun Ma, Gongliu Yang** Bifurcation control of guideway stick-slip motion with Washout filter. Transactions of Chinese Society of Agricultural Machinery, Vol. 39, Issue 11, 2008, p. 156-159.